PERGAMON

International Journal of Solids and Structures 38 (2001) 8481–8502

INTERNATIONAL JOURNAL OF SOLIDS and STRUCTURES

www.elsevier.com/locate/ijsolstr

A nonlinear analysis of the buckle propagation problem in deepwater pipelines

I.P. Pasqualino *, S.F. Estefen

Department of Ocean Engineering, COPPE, Federal University of Rio de Janeiro, P.O. Box 58608, 21945-970 Rio de Janeiro, Brazil

Received 28 December 1999; in revised form 19 April 2001

Abstract

A theoretical explicit formulation for numerical simulation of the buckle propagation in deepwater pipelines is proposed. It is based on thin shell theory incorporating large rotations and material elastic–plastic behavior for infinitesimal strains. The equilibrium equations are solved numerically through a computer program using the finite difference method associated to the dynamic relaxation technique. The pipe post-buckling behavior is determined by the arc-length method used in convolute regions of the load–displacement curve. The numerical results are correlated with experimental data from small scale laboratory tests. © 2001 Elsevier Science Ltd. All rights reserved.

Keywords: Buckle propagation; Submarine pipelines; Dynamic relaxation

1. Introduction

The buckle propagation in circular cylindrical shells under hydrostatic pressure is a post-buckling phenomenon causing a progressive structural failure. The collapse once initiated at a particular cross section of the cylindrical shell will propagate in both directions if the acting pressure is higher than a minimum value defined as the propagation pressure.

The possibility of buckle propagation in deepwater pipelines associated with limited availability of remote repair tools has contributed to conservative design approaches, based on the propagation pressure in damaged pipes, instead of the collapse pressure in intact pipes. It means thickness of approximately 1.5 to 2 times the values needed to resist the collapse of intact pipes. Therefore, the accurate prediction of the propagation pressure for deepwater pipelines contributes to less conservative design recommendations. It allows the designer to introduce the proper safety factors through reliability techniques considering the installation method and the risk involved.

The buckle propagation of pipelines was initially considered by Mesloh et al. (1973), but the first paper on the subject with a proposed equation for the propagation pressure was originated from an independent investigation by Palmer (1975) based on the strain energy of the collapsed cross-section. The results

* Corresponding author. Fax: +55-2-1562-7794.
E-mail address: ilson@lts.coppe.ufrj.br (I.P. Pasqualino).

PII: S0020-7683(01)00113-5

underestimated the experimental values for low ratios between external diameter and thickness (D/t), typical of deepwater scenarios where the effects of plastic deformations are predominant.

The first experimental studies were performed by Johns et al. (1976) and Mesloh et al. (1976) who tested different arrestors geometries used to stop the buckle propagation. Based on this study an empirical formula was proposed (Mesloh et al., 1976) to evaluate the propagation pressure (P_p) as a function of both D/t ratio and material yield stress (σ_0),

$$\frac{P_p}{\sigma_0} = 6\left(\frac{2t}{D}\right)^{2.5}. \tag{1}$$

Dynamic aspects of the propagation phenomenon were initially analyzed through experimental tests by Kyriakides and Babcock (1979), who later developed an empirical formulation to evaluate the efficiency of buckle arrestors (Kyriakides and Babcock, 1980a,b). An additional theoretical study (Kyriakides and Babcock, 1981) generated an empirical equation for the propagation pressure of aluminum and steel tubes, incorporating the material tangent modulus (E_t),

$$\frac{P_p}{\sigma_0} = \left[10.7 + 0.54\left(\frac{E_t}{\sigma_0}\right)\right]\left(\frac{t}{D}\right)^{2.25}. \tag{2}$$

A theoretical expression for the propagation pressure based on the internal energy dissipation of a simplified ring model was proposed by Steel and Spence (1983). The ring section was modeled with the aid of curved beam elements considering material strain hardening. Although they have presented good correlation with some experimental results, in general the proposed expression overestimated the propagation pressure,

$$\frac{P_p}{\sigma_0} = \frac{4}{\pi}\left(\frac{2t}{D}\right)^2\left[1.0 + 2.07\left(\frac{2t}{D}\right)^{0.35}\left(\frac{E_t}{\sigma_0}\right)^{0.12}\right]. \tag{3}$$

Kamalarasa and Calladine (1988) extended the Palmer approach to a three-dimensional model. A good correlation with experimental results was achieved but the proposed method requires experimental tests for the prediction of the propagation pressure.

Recently Estefen et al. (1996) carried out small scale experimental tests for deepwater pipelines in order to check the accuracy of the existing formulations. Eqs. (1) and (2) presented the best results.

Based on the analogy with the propagation phenomenon for inflated birthday balloons, Charter and Hutchinson (1984) developed a theoretical study to determine the propagation pressure using the balance between the dissipated energy and the deformation theory to describe the material plastic behavior. The proposed method underestimated the propagation pressures obtained experimentally, although the results were reasonable for D/t ratios higher than 30, due to the small effect of plasticity. In a contemporary and correlated work Kyriakides et al. (1984) proposed an expression for the propagation pressure from a more sophisticated numerical method. It was employed an incremental plasticity theory, but the bending strain energy in the tube axial direction was neglected. Again the obtained theoretical values underestimated the experimental results for D/t ratios less than 20.

Jensen (1988) conducted the first theoretical and numerical study for a three-dimensional solid to obtain the propagation pressure. The shell theory simplified by the Love–Kirchhoff approach for small strains and finite displacements associated with the material elastic–plastic flow theory was employed. Unfortunately no correlation with experimental results was presented.

Tassoulas et al. (1990) and Song and Tassoulas (1991) carried out three-dimensional analyses using the finite element method. Shell theory for finite displacements and strains associated with the flow theory with isotropic strain-hardening was employed. The loading unstable region was controlled by volume increments

and the external pressure was considered as an additional degree of freedom of the elements employed in the analysis. Correlation studies were successfully performed for D/t ratios higher than 35.

Dyau and Kyriakides (1993) presented a numerical analysis using the Rayleigh–Ritz method. The tube surface was modeled as thin shell, using the formulation proposed by Sanders (1963) for small strains and large displacements. Material behavior was described by the flow theory associated with isotropic strain hardening. Virtual work principle was used in an incremental form to obtain the system equilibrium integrals. The obtained results have shown good estimates for the propagation pressure as compared with experimental data from aluminum and steel small scale models with D/t ratios between 18 and 38. Good results were also obtained for the propagation pressure of tubes under tension loads (Kyriakides and Chang, 1992). A conclusive study on the propagating phenomenon in structures was published by Kyriakides (1994).

The buckle propagation problem has been modeled through implicit energy methods and analytical formulations. This paper proposes a new approach based on an explicit formulation associated with an innovative numerical solution technique for the equilibrium equations in the post-buckling regime. Considering that the thin shell theory has been employed the main aim is to obtain the propagation pressure for D/t ratios higher than 16, which represents a reasonable lower bound of the geometries that could be properly analyzed by this particular approach (Pasqualino, 1998).

2. Theoretical model

The theoretical model can be represented by a circular cylindrical shell with middle surface radius R, constant thickness t and length L. The shell geometry is defined by an orthogonal curvilinear coordinate system where x, θ and z correspond to axial, hoop and radial directions, respectively, as indicated in Fig. 1. A local Cartesian coordinate system x, y and z is employed to obtain the linear displacements u, v and w at a point P for instance, on the shell middle surface in the axial, hoop and radial directions, respectively.

The theoretical treatment of the propagation buckle of deepwater pipelines involves the consideration of both membrane and bending strains at the cross-sections as well as longitudinal strains in the regions between the pre- and post-buckling sections. Therefore, a three-dimensional model based on the thin shell theory as proposed by Sanders (1963) was employed. This theory is quite general, comprises finite displacements and finite strains within the Love–Kirchhoff assumptions.

The definition of the total strain and the general Sanders' kinematic relations are presented in Appendix A and B, respectively. The general thin shell equilibrium equations were modified to include the following forces effects and are presented in Appendix C. Assuming small strains, the shell general expressions were

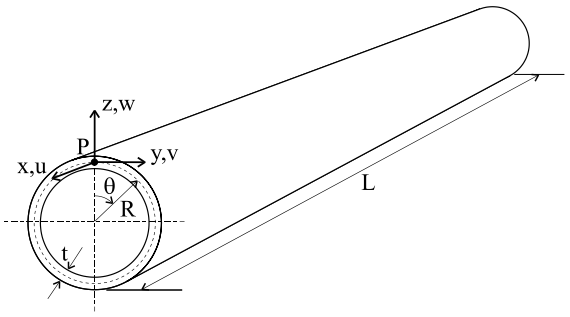

Fig. 1. Problem geometry.

simplified and specialized to the circular cylindrical shell geometry in order to establish the problem formulation.

2.1. Equilibrium equations

Five equilibrium equations deduced as described in Appendix C can be reduced to three, by substituting the bending moment equations into the force equations through the transverse shear stresses. These nonlinear equilibrium equations specialized to circular cylindrical shells subjected to a hydrostatic pressure p are presented in a general compact form, where the coefficient index i assumes the symbols x, θ and z concerning to the components in axial, hoop and radial directions, respectively,

$$\begin{aligned} &C_{i,1}N_{xx} + C_{i,2}N_{x\theta} + C_{i,3}N_{\theta\theta} + C_{i,4}M_{xx} + C_{i,5}M_{x\theta} + C_{i,6}M_{\theta\theta} + C_{i,7}\left(\frac{\partial N_{xx}}{\partial x} + \frac{1}{R}\frac{\partial N_{x\theta}}{\partial \theta}\right) \\ &\quad + C_{i,8}\left(\frac{\partial N_{x\theta}}{\partial x} + \frac{1}{R}\frac{\partial N_{\theta\theta}}{\partial \theta}\right) + C_{i,9}\left(\frac{\partial M_{xx}}{\partial x} + \frac{1}{R}\frac{\partial M_{x\theta}}{\partial \theta}\right) + C_{i,10}\left(\frac{\partial M_{x\theta}}{\partial x} + \frac{1}{R}\frac{\partial M_{\theta\theta}}{\partial \theta}\right) \\ &\quad + C_{i,11}\left(\frac{\partial^2 M_{xx}}{\partial x^2} + \frac{2}{R}\frac{\partial^2 M_{x\theta}}{\partial x\,\partial \theta} + \frac{1}{R^2}\frac{\partial^2 M_{\theta\theta}}{\partial \theta^2} - p\right) = 0, \end{aligned} \tag{4}$$

where

$$C_{x,1} = \frac{\partial^2 u}{\partial x^2}, \quad C_{\theta,1} = \frac{\partial^2 v}{\partial x^2}, \quad C_{z,1} = \frac{\partial^2 w}{\partial x^2},$$

$$C_{x,2} = \frac{2}{R}\frac{\partial^2 u}{\partial x\,\partial \theta}, \quad C_{\theta,2} = \frac{2}{R}\left(\frac{\partial^2 v}{\partial x\,\partial \theta} + \frac{\partial w}{\partial x}\right), \quad C_{z,2} = \frac{2}{R}\left(\frac{\partial^2 w}{\partial x\,\partial \theta} - \frac{\partial v}{\partial x}\right),$$

$$C_{x,3} = \frac{1}{R^2}\frac{\partial^2 u}{\partial \theta^2}, \quad C_{\theta,3} = \frac{1}{R^2}\left(\frac{\partial^2 v}{\partial \theta^2} + 2\frac{\partial w}{\partial \theta} - v\right), \quad C_{z,3} = \frac{1}{R^2}\left(\frac{\partial^2 w}{\partial \theta^2} - 2\frac{\partial v}{\partial \theta} - w\right) - \frac{1}{R},$$

$$C_{x,4} = \frac{\partial^2 u}{\partial x^2}K_{xx} + \frac{1}{R}\frac{\partial^2 u}{\partial x\,\partial \theta}K_{x\theta} + \left(1 + \frac{\partial u}{\partial x}\right)\frac{\partial K_{xx}}{\partial x} + \frac{1}{R}\frac{\partial u}{\partial \theta}\frac{\partial K_{x\theta}}{\partial x},$$

$$C_{\theta,4} = \frac{\partial^2 v}{\partial x^2}K_{xx} + \frac{1}{R}\left(\frac{\partial^2 v}{\partial x\,\partial \theta} + \frac{\partial w}{\partial x}\right)K_{x\theta} + \frac{\partial v}{\partial x}\frac{\partial K_{xx}}{\partial x} + \left[1 + \frac{1}{R}\left(\frac{\partial v}{\partial \theta} + w\right)\right]\frac{\partial K_{x\theta}}{\partial x},$$

$$C_{z,4} = \frac{\partial^2 w}{\partial x^2}K_{xx} + \frac{1}{R}\left(\frac{\partial^2 w}{\partial x\,\partial \theta} - \frac{\partial v}{\partial x}\right)K_{x\theta} + \frac{\partial w}{\partial x}\frac{\partial K_{xx}}{\partial x} + \frac{1}{R}\left(\frac{\partial w}{\partial \theta} - v\right)\frac{\partial K_{x\theta}}{\partial x},$$

$$\begin{aligned} C_{x,5} = {} & \frac{1}{R}\frac{\partial^2 u}{\partial x\,\partial \theta}\left(K_{xx} + K_{\theta\theta} + \frac{1}{R}\right) + \left(\frac{\partial^2 u}{\partial x^2} + \frac{1}{R^2}\frac{\partial^2 u}{\partial \theta^2}\right)K_{x\theta} + \left(1 + \frac{\partial u}{\partial x}\right)\left(\frac{\partial K_{x\theta}}{\partial x} + \frac{1}{R}\frac{\partial K_{xx}}{\partial \theta}\right) \\ & + \frac{1}{R}\frac{\partial u}{\partial \theta}\left(\frac{\partial K_{\theta\theta}}{\partial x} + \frac{1}{R}\frac{\partial K_{x\theta}}{\partial \theta}\right), \end{aligned}$$

$$\begin{aligned} C_{\theta,5} = {} & \frac{1}{R}\left(\frac{\partial^2 v}{\partial x\,\partial \theta} + \frac{\partial w}{\partial x}\right)\left(K_{xx} + K_{\theta\theta} + \frac{1}{R}\right) + \left[\frac{\partial^2 v}{\partial x^2} + \frac{1}{R^2}\left(\frac{\partial^2 v}{\partial \theta^2} + 2\frac{\partial w}{\partial \theta} - v\right)\right]K_{x\theta} \\ & + \frac{\partial v}{\partial x}\left(\frac{\partial K_{x\theta}}{\partial x} + \frac{1}{R}\frac{\partial K_{xx}}{\partial \theta}\right) + \left[1 + \frac{1}{R}\left(\frac{\partial v}{\partial \theta} + w\right)\right]\left(\frac{\partial K_{\theta\theta}}{\partial x} + \frac{1}{R}\frac{\partial K_{x\theta}}{\partial \theta}\right), \end{aligned}$$

$$C_{z,5} = \frac{1}{R}\left(\frac{\partial^2 w}{\partial x\,\partial\theta} - \frac{\partial v}{\partial x}\right)\left(K_{xx} + K_{\theta\theta} + \frac{1}{R}\right) + \left[\frac{\partial^2 w}{\partial x^2} + \frac{1}{R^2}\left(\frac{\partial^2 w}{\partial\theta^2} - 2\frac{\partial v}{\partial\theta} - w - R\right)\right]K_{x\theta} + \frac{\partial w}{\partial x}\left(\frac{\partial K_{x\theta}}{\partial x} + \frac{1}{R}\frac{\partial K_{xx}}{\partial\theta}\right) + \frac{1}{R}\left(\frac{\partial w}{\partial\theta} - v\right)\left(\frac{\partial K_{\theta\theta}}{\partial x} + \frac{1}{R}\frac{\partial K_{x\theta}}{\partial\theta}\right),$$

$$C_{x,6} = \frac{1}{R^2}\frac{\partial^2 u}{\partial\theta^2}\left(K_{\theta\theta} + \frac{1}{R}\right) + \frac{1}{R}\frac{\partial^2 u}{\partial x\,\partial\theta}K_{x\theta} + \frac{1}{R}\left(1 + \frac{\partial u}{\partial x}\right)\frac{\partial K_{x\theta}}{\partial\theta} + \frac{1}{R^2}\frac{\partial u}{\partial\theta}\frac{\partial K_{\theta\theta}}{\partial\theta},$$

$$C_{\theta,6} = \frac{1}{R^2}\left(\frac{\partial^2 v}{\partial\theta^2} + 2\frac{\partial w}{\partial\theta} - v\right)\left(K_{\theta\theta} + \frac{1}{R}\right) + \frac{1}{R}\left(\frac{\partial^2 v}{\partial x\,\partial\theta} + \frac{\partial w}{\partial x}\right)K_{x\theta} + \frac{1}{R}\frac{\partial v}{\partial x}\frac{\partial K_{x\theta}}{\partial\theta} + \left[1 + \frac{1}{R}\left(\frac{\partial v}{\partial\theta} + w\right)\right]\frac{1}{R}\frac{\partial K_{\theta\theta}}{\partial\theta},$$

$$C_{z,6} = \frac{1}{R^2}\left(\frac{\partial^2 w}{\partial\theta^2} - 2\frac{\partial v}{\partial\theta} - w - R\right)\left(K_{\theta\theta} + \frac{1}{R}\right) + \frac{1}{R}\left(\frac{\partial^2 w}{\partial x\,\partial\theta} - \frac{\partial v}{\partial x}\right)K_{x\theta} + \frac{1}{R}\frac{\partial w}{\partial x}\frac{\partial K_{x\theta}}{\partial\theta} + \frac{1}{R^2}\left(\frac{\partial w}{\partial\theta} - v\right)\frac{\partial K_{\theta\theta}}{\partial\theta},$$

$$C_{x,7} = \left(1 + \frac{\partial u}{\partial x}\right), \quad C_{\theta,7} = \frac{\partial v}{\partial x}, \quad C_{z,7} = \frac{\partial w}{\partial x},$$

$$C_{x,8} = \frac{1}{R}\frac{\partial u}{\partial\theta}, \quad C_{\theta,8} = 1 + \frac{1}{R}\left(\frac{\partial v}{\partial\theta} + w\right), \quad C_{z,8} = \frac{1}{R}\left(\frac{\partial w}{\partial\theta} - v\right),$$

$$C_{x,9} = \left(1 + \frac{\partial u}{\partial x}\right)K_{xx} + \frac{1}{R}\frac{\partial u}{\partial\theta}K_{x\theta} + \frac{\partial N_1}{\partial x},$$

$$C_{\theta,9} = \frac{\partial v}{\partial x}K_{xx} + \left[1 + \frac{1}{R}\left(\frac{\partial v}{\partial\theta} + w\right)\right]K_{x\theta} + \frac{\partial N_2}{\partial x},$$

$$C_{x,9} = \frac{\partial w}{\partial x}K_{xx} + \frac{1}{R}\left(\frac{\partial w}{\partial\theta} - v\right)K_{x\theta} + \frac{\partial N_3}{\partial x},$$

$$C_{x,10} = \left(1 + \frac{\partial u}{\partial x}\right)K_{x\theta} + \frac{1}{R}\frac{\partial u}{\partial\theta}\left(K_{\theta\theta} + \frac{1}{R}\right) + \frac{1}{R}\frac{\partial N_1}{\partial\theta},$$

$$C_{\theta,10} = \frac{\partial v}{\partial x}K_{x\theta} + \left[1 + \frac{1}{R}\left(\frac{\partial v}{\partial\theta} + w\right)\right]\left(K_{\theta\theta} + \frac{1}{R}\right) + \frac{1}{R}\left(\frac{\partial N_2}{\partial\theta} + N_3\right),$$

$$C_{z,10} = \frac{\partial w}{\partial x}K_{x\theta} + \frac{1}{R}\left(\frac{\partial w}{\partial\theta} - v\right)\left(K_{\theta\theta} + \frac{1}{R}\right) + \frac{1}{R}\left(\frac{\partial N_3}{\partial\theta} - N_2\right),$$

$$C_{x,11} = N_1, \quad C_{\theta,11} = N_2, \quad C_{z,11} = N_3.$$

The tensor $K_{\alpha\beta}$ and the vector N_i represent the bending strains and the normal unit vector to the deformed middle surface, respectively (see Appendix B). The modified symmetric tensors in Eq. (4), $N_{\alpha\beta}$ and $M_{\alpha\beta}$, represent the membrane forces and bending moments, respectively. They are related to the contravariant non symmetric resultant tensors ${}^0N^{\alpha\beta}$ and ${}^0M^{\alpha\beta}$ through the following relations proposed by Sanders (1963):

$$N^{\alpha\beta} = {}^0N^{\alpha\beta} - B^{\beta}_{\gamma}\,{}^0M^{\gamma\alpha} \tag{5}$$

and

$$M^{\alpha\beta} = \frac{1}{2}({}^0M^{\alpha\beta} + {}^0M^{\beta\alpha}). \tag{6}$$

2.2. Constitutive relations

The membrane stress and bending moment resultants for small strains and finite rotations are given by the integrals

$${}^0N^{\alpha\beta} = \int_{-t/2}^{t/2} \sqrt{\frac{g}{a}}(\delta^{\beta}_{\gamma} + zB^{\beta}_{\gamma})\sigma^{\alpha\gamma}\,\mathrm{d}z \tag{7}$$

and

$${}^0M^{\alpha\beta} = \int_{-t/2}^{t/2} \sqrt{\frac{g}{a}}(\delta^{\beta}_{\gamma} + zB^{\beta}_{\gamma})\sigma^{\alpha\gamma} z\,\mathrm{d}z, \tag{8}$$

where δ^{β}_{γ} is the mixed tensor Kronecker delta, $\sigma^{\alpha\gamma}$ is the contravariant stress tensor, g and a are the determinants of the metric tensors $g_{\alpha\beta}$ and $a_{\alpha\beta}$ of the undeformed shell and shell middle surface, respectively. Adapting Eqs. (7) and (8) for cylindrical coordinates the integrals defining force and moment resultants per unit length of the deformed shell middle surface can be obtained,

$${}^0N_{xx} = \int_{-t/2}^{t/2} \left(1 + \frac{z}{R}\right)[(1 + zK_{xx})\sigma_{xx} + zK_{x\theta}\sigma_{x\theta}]\,\mathrm{d}z, \tag{9}$$

$${}^0N_{\theta\theta} = \int_{-t/2}^{t/2} \left[\left(1 + \frac{z}{R} + zK_{\theta\theta}\right)\sigma_{\theta\theta} + zK_{x\theta}\sigma_{x\theta}\right] \Big/ \left(1 + \frac{z}{R}\right) \mathrm{d}z, \tag{10}$$

$${}^0N_{x\theta} = \int_{-t/2}^{t/2} \left(1 + \frac{z}{R} + zK_{\theta\theta}\right)\sigma_{x\theta} + zK_{x\theta}\sigma_{xx}\,\mathrm{d}z, \tag{11}$$

$${}^0N_{\theta x} = \int_{-t/2}^{t/2} (1 + zK_{xx})\sigma_{x\theta} + zK_{x\theta}\sigma_{\theta\theta}\,\mathrm{d}z, \tag{12}$$

$${}^0M_{xx} = \int_{-t/2}^{t/2} \left(1 + \frac{z}{R}\right)[(1 + zK_{xx})\sigma_{xx} + zK_{x\theta}\sigma_{x\theta}]z\,\mathrm{d}z, \tag{13}$$

$${}^0M_{\theta\theta} = \int_{-t/2}^{t/2} \left\{\left[\left(1 + \frac{z}{R} + zK_{\theta\theta}\right)\sigma_{\theta\theta} + zK_{x\theta}\sigma_{x\theta}\right] \Big/ \left(1 + \frac{z}{R}\right)\right\} z\,\mathrm{d}z, \tag{14}$$

$${}^0M_{x\theta} = \int_{-t/2}^{t/2} \left[\left(1 + \frac{z}{R} + zK_{\theta\theta}\right)\sigma_{x\theta} + zK_{x\theta}\sigma_{xx}\right] z\,\mathrm{d}z \tag{15}$$

and

$$^{0}M_{\theta x} = \int_{-t/2}^{t/2} [(1 + zK_{xx})\sigma_{x\theta} + zK_{x\theta}\sigma_{\theta\theta}]z\,\mathrm{d}z. \tag{16}$$

2.3. Plasticity

In the material elastic–plastic regime the stress–strain relations are obtained from a theoretical model incorporating the potential and associated flow law, small strains and the Von Mises yield criterion with isotropic strain hardening.

Considering plane stresses and a scalar hardening law, the Von Mises yield function (f) is defined in this case by the equation

$$f = \sqrt{\sigma_{xx}^2 + \sigma_{\theta\theta}^2 - \sigma_{xx}\sigma_{\theta\theta} + 3\sigma_{x\theta}^2} - (H + \sigma_0), \tag{17}$$

where σ_0 is the yield stress and H is a scalar function of the equivalent plastic strain $\varepsilon_{\mathrm{eqv}}^{\mathrm{p}}$ representing the increase of stress in relation to the undeformed material.

The relation between the stress (σ) and the strain (ε) tensors in the elastic–plastic regime is given by the expressions

$$\dot{\sigma} = \boldsymbol{C}_{\mathrm{t}} : \dot{\varepsilon} \tag{18}$$

and

$$\boldsymbol{C}_{\mathrm{t}} = \boldsymbol{C} - \frac{\boldsymbol{C} : \boldsymbol{a} \otimes \boldsymbol{a} : \boldsymbol{C}}{\boldsymbol{a} : \boldsymbol{C} : \boldsymbol{a} + h}, \tag{19}$$

where $\boldsymbol{C}_{\mathrm{t}}$ is the tangent modular matrix, the symbols (:) and ($\otimes$) mean, respectively, inner and tensor products and the dot ($^{\bullet}$) can be simply considered as small changes. The tensor $\boldsymbol{C}$ is the elastic matrix for plane stress assuming isotropic elasticity. The tensor $\boldsymbol{a}$ is normal to yield surface and calculated from $\boldsymbol{a} = \partial f/\partial\sigma$ and h is the hardening parameter given by:

$$h = \frac{\partial H}{\partial \varepsilon_{\mathrm{eqv}}^{\mathrm{p}}}. \tag{20}$$

3. Numerical method

The equilibrium equations are solved numerically using an iterative vectorial technique called dynamic relaxation (Underwood, 1983) combined with the finite difference method. The dynamic relaxation technique transforms a static problem in a dynamic one by adding both fictitious densities and critical damping. The use of the finite difference method avoids matrix operations and allows the vectorial arrangement of the equation system contributing to save computer space memory and to simplify the numerical formulation. A technique based on the arc-length method as proposed by Riks (1979) is employed to obtain the unstable equilibrium configurations in the post-buckling regime.

3.1. Dynamic relaxation

The technique consists of obtaining the static solution from the transient response of a system excited through a suddenly loading. The dynamic equilibrium equations corresponding to n degrees of freedom of

the system are solved for a damping coefficient close to the critical one. After some initial oscillations both velocities and accelerations tend to zero while the vector of displacements approaches to the deformed equilibrium configuration. The method is normally used for the solution of problems with high nonlinear geometry and material behavior, including ultimate strength analyses with structural unloading.

3.1.1. Finite difference mesh

Superimposed finite difference meshes (Fig. 2) are adopted in order to increase the accuracy of the first order derivatives. The problem unknowns are calculated for specific meshes and then linearly interpolated to the others if necessary. The main mesh is used to calculate the radial displacements w, the normal strains components ε_{xx} and $\varepsilon_{\theta\theta}$, the normal forces N^0_{xx} and $N^0_{\theta\theta}$ and the bending moments M^0_{xx} and $M^0_{\theta\theta}$. The secondary mesh is used to calculate the shear strain component $\varepsilon_{x\theta}$, shear forces $N^0_{x\theta}$ and $N^0_{\theta x}$ and the shear moments $M^0_{x\theta}$ and $M^0_{\theta x}$. The additional meshes define the nodes where the equilibrium equations for the displacements u and v are solved.

The proposed finite difference meshes are generated over 1/8 of the pipe surface, as presented in Fig. 3, since the planes XY, XZ and YZ are assumed to be planes of symmetry. Mesh spacing in axial (Δx) and hoop ($\Delta\theta$) directions are constants and defined by the variables NMX and NMY, respectively. The pipe structure is defined between the nodes $I = 2$ and $I =$ NMX2 in axial direction and the nodes $J = 2$ and $J =$ NMY2 in hoop direction. The fictitious nodes $I = 1$, NMX3 and $J = 2$, NMY2 are used to define the boundary conditions.

3.1.2. Method formulation

The dynamic relaxation technique is based on the time domain integration of the following equations related to the kth time increment to obtain the discrete displacement vector $\boldsymbol{q}$:

$$\dot{\boldsymbol{q}}^{k+1/2} = \frac{(2 - c\Delta t)}{(2 + c\Delta t)}\dot{\boldsymbol{q}}^{k-1/2} + \frac{2\boldsymbol{M}^{-1}\boldsymbol{r}^k\Delta t}{(2 + c\Delta t)} \tag{21}$$

and

$$\boldsymbol{q}^{k+1} = \boldsymbol{q}^k + \dot{\boldsymbol{q}}^{k+1/2}\Delta t, \tag{22}$$

where $\boldsymbol{M}$ is a mass diagonal matrix ($n \times n$), $\boldsymbol{r}$ the residual vector, c the damping coefficient and the dot ($\bullet$) means derivative in relation to the time t. The residual force vector is given by

$$\boldsymbol{r}^k = \boldsymbol{P}^k - \boldsymbol{F}^k_{\text{int}}, \tag{23}$$

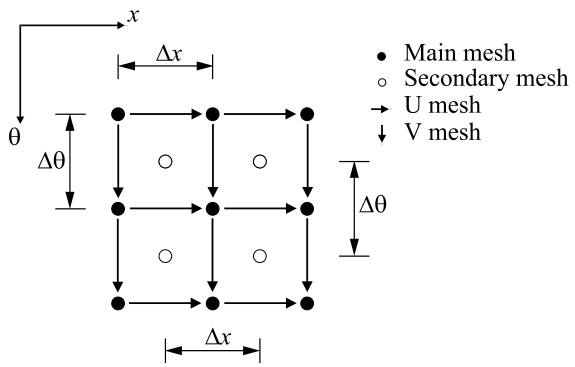

Fig. 2. Superimposed meshes.

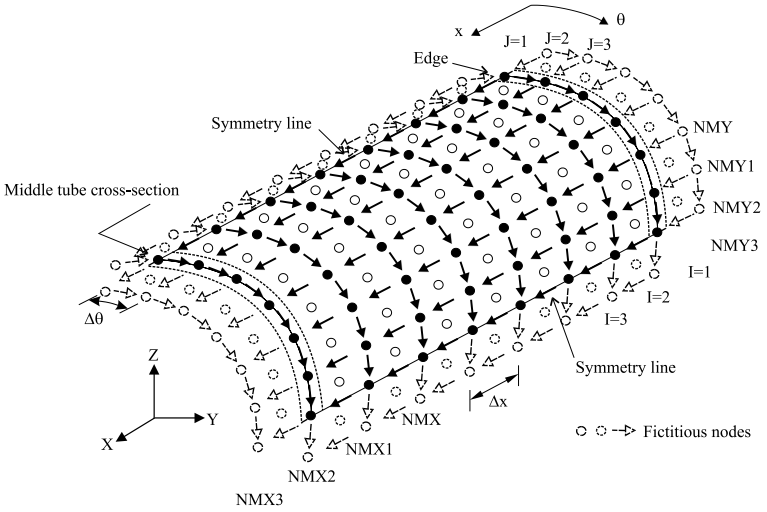

Fig. 3. Finite difference mesh for the numerical model.

where $\boldsymbol{F}_{\text{int}}$ is the internal force vector and $\boldsymbol{P}$ the external load vector. When the velocity vector $\dot{\boldsymbol{q}}$ approaches zero the static equilibrium is then assumed,

$$\boldsymbol{F}_{\text{int}}^{k} - \boldsymbol{P}^{k} = 0. \tag{24}$$

The parameters c, $\boldsymbol{M}$ and Δt must be chosen such as to obtain optimum performance and numerical stability. A damping coefficient close to the critical one can speed up the convergence that is obtained when $\boldsymbol{r}^{k} \approx 0$.

3.1.3. Parameters c, Mand Δt

The procedure to obtain adequate convergence parameters was based on a detailed study developed by Underwood (1983). The use of fictitious densities accelerates the convergence of the algorithm and guarantees its numerical stability. The time increment Δt is given by the inequality below:

$$\Delta t \leqslant \frac{2}{\sqrt{A_{\text{m}}}}, \tag{25}$$

where A_{m} is the highest eigenvalue of the matrix $\boldsymbol{A}$, defined by $\boldsymbol{A} = \boldsymbol{M}^{-1}\boldsymbol{K}$ and $\boldsymbol{K}$ is the implicit rigidity matrix of the finite difference method. Using the Gerschgörin theorem to establish the upper bound of the highest eigenvalue, the lower bound of the fictitious densities (m_{ii}) can be defined as (Cassel and Hobbs, 1976),

$$m_{ii} \geqslant \frac{1}{4}\Delta t^{2} \sum_{j=1}^{n} |k_{ij}|. \tag{26}$$

Evaluating the diagonal matrix $\boldsymbol{M}$ with $\Delta t = 1.1$ in Eq. (26) and iterating Eqs. (21) and (22) with $\Delta t = 1.0$ a good margin to ensure stability is provided.

The damping coefficient c is obtained every iteration through the following expression based on the Rayleigh quotient,

$$c = \sqrt{\boldsymbol{q}^{T\,1}\boldsymbol{K}\boldsymbol{q}/\boldsymbol{q}^{T\,1}\boldsymbol{M}\boldsymbol{q}}, \tag{27}$$

where the diagonal matrix ${}^1\boldsymbol{K}$, known as the local rigidity matrix, has the elements calculated in each iteration by

$$ {}^1\boldsymbol{K}^k = [-\boldsymbol{F}_{\text{int}}^{k-1} + \boldsymbol{F}_{\text{int}}^{k}]/\Delta t\dot{\boldsymbol{q}}^{k-1/2}. \tag{28} $$

3.1.4. Numerical procedure

The problem is solved incrementally with small load steps in order to update the geometry and material properties. The kinematic, total strain, constitutive and equilibrium equations are used in the incremental form and the partial derivatives are approximated with the aid of the finite difference expressions. In an iterative process, the incremental equations are evaluated at each node of the finite difference meshes in order to reach the convergence of the recursive equations (21) and (22) for the prescribed increment of pressure (δp).

Considering a degree of freedom i of the main mesh, for instance, Eqs. (21) and (22) assume the particular form

$$ \dot{w}_i^{k+1/2} = \frac{(2 - c\Delta t)}{(2 + c\Delta t)}\dot{w}_i^{k-1/2} + \frac{2r_{z,i}^k \Delta t}{m_{ii}(2 + c\Delta t)} \tag{29} $$

and

$$ \delta w_i^{k+1} = \delta w_i^k + \dot{w}_i^{k+1/2}\Delta t, \tag{30} $$

where the residual component $r_{z,i}^k$ corresponds to the equilibrium equation (4) in the z direction calculated at the degree of freedom i and iteration k.

The incremental stress–strain relations are needed to evaluate the constitutive equations in the elastic–plastic regime. Since the Eq. (18) deals with infinitesimal changes of stress and strain, it is not appropriate to be directly applied in a numerical procedure where finite increments of stress and strain must be related to each other. It would lead to stress states out of the yield surface, which is theoretically inconsistent. To overcome this problem a numerical procedure called "Backward Euler Return" (Crisfield, 1991), which iteratively provides the return to the yield surface, was incorporated into the plasticity routine. It replaces the tangent modular matrix by the consistent tangent modular matrix $\boldsymbol{C}_{\text{tc}}$, which is obtained iteratively and leads to the following relation:

$$ \begin{bmatrix} \delta\sigma_{xx} \\ \delta\sigma_{\theta\theta} \\ \delta\sigma_{x\theta} \end{bmatrix} = \begin{bmatrix} C_{\text{tc11}} & C_{\text{tc12}} & C_{\text{tc13}} \\ C_{\text{tc21}} & C_{\text{tc22}} & C_{\text{tc23}} \\ C_{\text{tc31}} & C_{\text{tc32}} & C_{\text{tc33}} \end{bmatrix} \begin{bmatrix} \delta\varepsilon_{xx} \\ \delta\varepsilon_{\theta\theta} \\ 2\delta\varepsilon_{x\theta} \end{bmatrix}. \tag{31} $$

The yield function is verified at the end of each load step on main and secondary meshes at eleven points along the thickness. The consistent matrix is evaluated where yield occurs, otherwise, the elastic matrix $\boldsymbol{C}$ is considered. The Eq. (31) is substituted in the incremental constitutive equations and the coefficients of $\boldsymbol{C}_{\text{tc}}$ are numerically integrated through the shell thickness.

3.2. Arc-length method

The arc-length method was first introduced by Riks (1970) and used by Wempner (1971) in order to facilitate the incremental computations near limit points. Riks (1979) published one of the most representative studies related to the method. Ramesh and Krishnamoorthy (1993) applied the method for the first time in association with the dynamic relaxation technique to obtain the load–displacement history in the post-buckling regime. A constrain condition based on the norm of the total displacements discrete vector was employed. After being tested, the proposed condition showed to be inadequate to determine the

post-buckling behavior of shells. The incremental solution procedure resulted in an oscillating response for the unstable region of the equilibrium path.

In this paper the method is used to calculate the load increment (δp) that becomes an unknown in the unstable region of the equilibrium path. It consists of the addition of a constrain condition to the n equilibrium equations to obtain the solution of $n+1$ unknowns, the n degrees of freedom and an incremental load intensity factor $\delta\Lambda$. The circular constrain condition proposed by Crisfield (1981) was considered adequate to be employed in the dynamic relaxation technique,

$$\|\delta \boldsymbol{q}^{k+1}\|^2 + (\delta\Lambda^{k+1})^2 = S^2, \tag{32}$$

where S means the arc-length.

Considering that the external loading is represented only by the variable p, which is the hydrostatic pressure in the present case, the acting load is defined as a function of a constant reference value p_{ref} given by the expression

$$p^k = \Lambda^{k+1} p_{\text{ref}}. \tag{33}$$

Employing the incremental form of Eqs. (21) and (22) in Eq. (32), the constrain condition is represented with the aid of a second degree polynomial equation,

$$a_1(\delta\Lambda_m^{k+1})^2 + a_2\delta\Lambda_m^{k+1} + a_3 = 0, \tag{34}$$

where the coefficients are given as functions of the problem parameters. If the discriminant of Eq. (34) is positive, two real roots ($^1\delta\Lambda$ and $^2\delta\Lambda$) will be obtained. In order to determine the correct root, new incremental displacement vectors ($^1\delta\boldsymbol{q}$ and $^2\delta\boldsymbol{q}$) must be calculated using the obtained roots, so that the cosine of the angles formed between these vectors and the former solution can be estimated. The correct root is that responsible for the smallest angle, i.e., the highest cosine value.

The use of the arc-length method to determine the load increments δp in the dynamic relaxation technique is relatively simple. The analysis is initiated with prescribed load increments according to the numerical procedure presented in Section 3.1.4. Then the parameter S in Eq. (32) can be evaluated from the known values of $\delta\boldsymbol{q}$ and $\delta\Lambda$, determined from the last load step without the arc-length method control. When it starts, the expression (34) is calculated at the end of the iterations to obtain the correct root, which is employed in the incremental form of Eq. (33) to define the pressure increment to the next iteration. The load step is concluded when convergence is reached for the δp value.

3.3. Loading control

Buckling analysis of circular cylindrical shells under external pressure must incorporate geometrical imperfections, so that the tube cross-section can configure the characteristic failure mode. Here, the initial displacements (w_0) are made equal to

$$w_0 = w_{\max}\cos(2\theta), \tag{35}$$

where $w_{\max}$ is the maximum initial geometric imperfection, assumed as $w_{\max} = R\Delta_0$ and Δ_0 is the initial cross-section ovalization which may vary along the pipe length.

The collapse must be localized at the pipe middle cross-section in order to simulate the buckle propagation. This is accomplished by assuming a larger ovalization at the pipe middle cross-section and a constant smaller one along the rest of the pipe length. The larger prescribed initial displacements of the middle section will localize the buckle at this region at a pressure level called initiation collapse pressure (P_i). An initial estimative of P_i may be obtained from a trial analysis of the buckling pressure with the mentioned larger initial displacements made constant over the entire pipe.

The quasi-static buckle propagation analyses may be divided in three phases and the related procedures are presented hereafter.

3.3.1. Phase 1

The pressure increments are prescribed until $0.75P_i$ so that the parameter S in Eq. (32) may be defined. This stage represents the stable behavior of the structure where the increments converge quickly. Later, the arc-length routine starts controlling the applied load by determining δp from the defined arc increments. Considering the imperfection distribution adopted, the first yield occurs at the node located at the middle cross-section and coordinate $\theta = 0$ ($I = \mathrm{NMX2}$ and $J = 2$ according to Fig. 3). After the pipe collapse, calculated negative values of δp reduce the overall applied external pressure.

3.3.2. Phase 2

This phase is related to the structure post-buckling behavior where the arc-length routine keeps calculating negative pressure increments. It is finished when the middle cross-section internal faces touch each other. Due to the initial imperfection distribution adopted, the degrees of freedom $w(\mathrm{NMX2}, 2)$ registers the first contact, being prescribed afterwards with the value $-R + t/2$.

3.3.3. Phase 3

As soon as the first nodes contact is registered, the arc-length routine starts calculating positive pressure increments, raising the overall applied pressure to define a plateau that configures the propagation pressure. The computational program is provided with a contact routine that verifies at each load step if any node has reached the longitudinal symmetry plane. The nodes that register contact have their degrees of freedom prescribed and are again excluded from the algorithm. The longitudinal line defined by the degrees of freedom $w(I, 2)$, where $I = 2, \ldots, \mathrm{NMX2}$, is a reference to control the model propagation process.

4. Correlation between numerical and experimental results

Results from numerical analyses and quasi-static buckle propagation tests are correlated in order to verify the proposed methodology.

4.1. Laboratory tests

Six laboratory tests using small scale steel models with D/t ratios equal to 16, 21 and 24 were selected from Estefen et al. (1996) for the correlation study on buckle propagation.

The models were made up with length to external diameter ratio (L/D) of 60, providing the length required for the propagating collapse configuration and end plug fittings. Table 1 provides the material mechanical properties obtained through uniaxial tensile tests of specimens cut from the original tubes. To initiate the buckle under external pressure, the models were damaged with the aid of a frame provided with

Table 1
Mechanical and geometrical properties for the small scale models

Model	R (mm)	t (mm)	σ_0 (N/mm^2)	E_t (N/mm^2)
TSP16A	18.75	2.50	342.00	2550.78
TSP16B	18.75	2.50	295.20	1364.21
TSP21A	20.00	2.00	228.58	613.33
TSP21B	20.00	2.00	281.03	453.44
TSP24A	24.35	2.10	452.93	1004.06
TSP24B	24.35	2.10	326.51	697.68

a hydraulic actuator. Depth damages were about 60% of the respective model external diameters to enforce that initiation and propagation pressures would have similar values.

The test procedure consisted of gradual pressurization in the hyperbaric chamber until the model initiation collapse pressure, leading to a sudden drop of the chamber pressure to levels below the model propagation pressure. Then, small pressure increments were applied in order to raise the chamber pressure to a constant level in which the buckle propagated slowly, establishing a plateau for the model propagation pressure.

4.2. Numerical analyses

Quasi-static buckle propagation analyses were simulated by the computer program using data from the small scale models presented in Table 1. Numerical analyses were carried out in the computer system Cray J90. The finite difference main mesh was generated with a half length equal to $12D$, hoop and axial meshing spacing equal to 6 and 45, respectively, adopting the symmetry conditions described in Section 3.1.1. The axial mesh spacing is automatically set by the numerical program as equal to twice the hoop mesh spacing.

The mesh refinement was checked with the aid of a sensitivity analysis of buckling pressure for an intact pipe. For this purpose it was employed a steel pipe model ($D/t = 16$; $\Delta_0 = 0.00177$; $\sigma_0 = 280.8$ N/mm^2) with experimental collapse pressure equal to 43.47 N/mm^2 (Estefen and Aguiar, 1994). Different mesh refinements were examined with the hoop mesh spacing varying from 6 to 9, considering a model half length equal to $7.5D$. According to Table 2, the results of numerical collapse pressure $\overline{P}_c$ presented reduced sensitivity to the mesh refinements considered. Therefore, the hoop mesh spacing equal to six were used for the buckle propagation analyses.

The propagation pressure was determined after the complete closure of twelve cross-sections along half tube. The buckle propagation configuration for half tube is presented in Fig. 4, where it can be verified that

Table 2
Numerical collapse pressures for mesh refinement analyses

N° of axial divisions	N° of hoop divisions	$\overline{P}_c$ (N/mm^2)
28	6	42.09
33	7	42.10
38	8	42.12
43	9	42.14

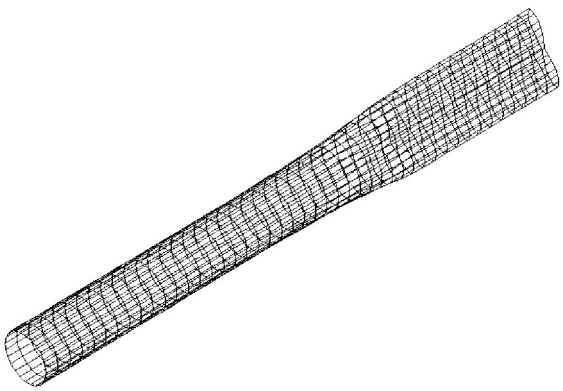

Fig. 4. Configuration of the buckle propagation for half tube.

the employed buckle localization procedure was very efficient. The cross-sections far from the tube middle section were not affected by the external pressure. The behavior of the numerical models during buckle propagation analyses is better understood with the aid of Figs. 5–10, which represent the load intensity factor Λ versus the discrete displacement vector norm $\boldsymbol{q}$ for six small scale models. All the phases of the numerical process and the propagation pressure can be visualized through these curves. It can be verified that the acting external pressure was incremented from zero to a maximum value corresponding to the initiation collapse pressure. Later, negative incremental pressures were added until the tube internal faces touch each other. In the last phase, the acting external pressure was increased up to the propagation pressure plateau. Table 3 presents both experimental $\hat{P}_p$ and numerical $\overline{P}_p$ results of the propagation pressure models and the respective differences in relation to the experimental results. The numerical results were graphically obtained from the plotted curves in Figs. 5–10 which also present the propagation pressure plateau defined by the experimental tests.

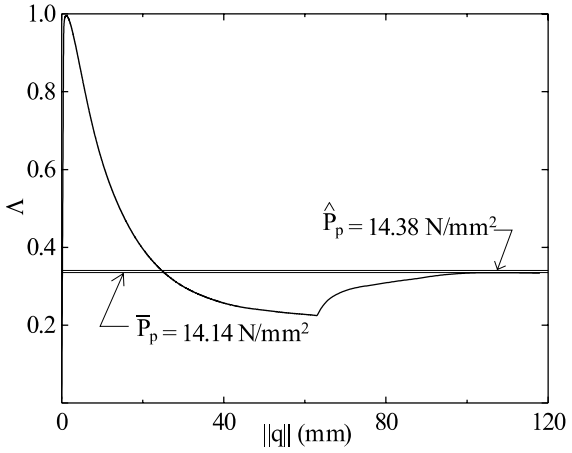

Fig. 5. Load intensity factor versus displacement vector norm of model TSP16A.

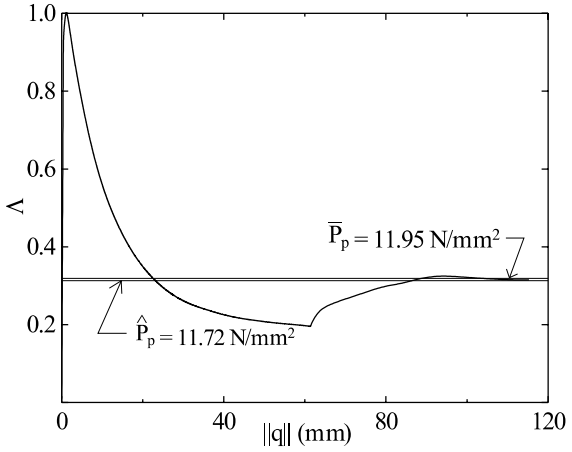

Fig. 6. Load intensity factor versus displacement vector norm of model TSP16B.

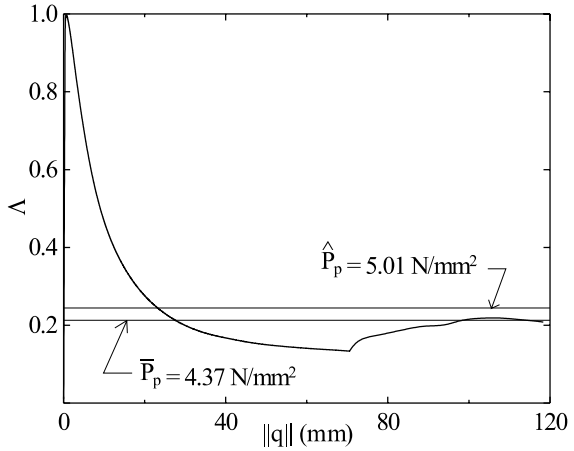

Fig. 7. Load intensity factor versus displacement vector norm of model TSP21A.

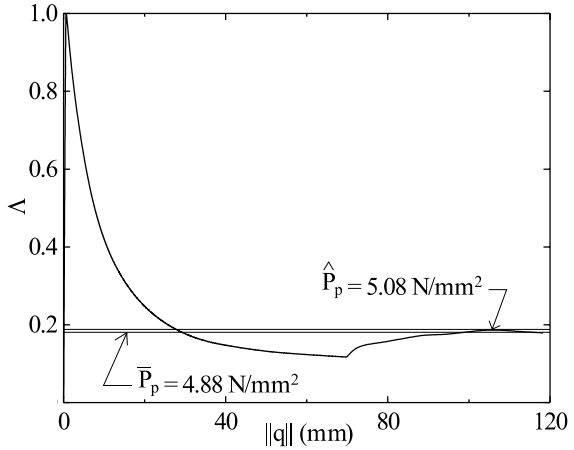

Fig. 8. Load intensity factor versus displacement vector norm of model TSP21B.

The analyses showed good correlation between numerical and experimental results validating the theoretical model and the proposed numerical technique. Better numerical results could be probably obtained if additional material properties data for the tested models were available. These results showed to be highly dependent on the material stress–strain curves from uniaxial tensile tests. Discrepancies between numerical and experimental results have not presented tendency to either underestimate or overestimate the propagation pressure predictions. Good results were obtained through all analyzed D/t ratios, which demonstrated that the theory considered is appropriate to lower bound D/t ratio equal to 16.

The mesh refinement and model length showed to be correctly defined to obtain the propagation pressure plateau. If the model were too short, the constant pressure plateau would not be properly obtained due to the boundary condition effect. The model length reserved to configure the buckle propagation, equal to three times the respective diameter, was large enough to define the propagation pressure.

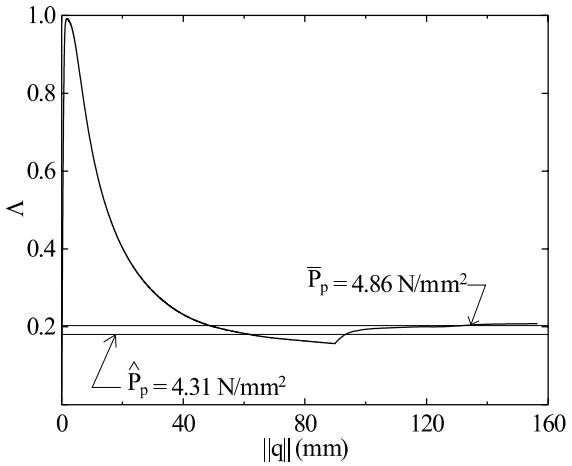

Fig. 9. Load intensity factor versus displacement vector norm of model TSP24A.

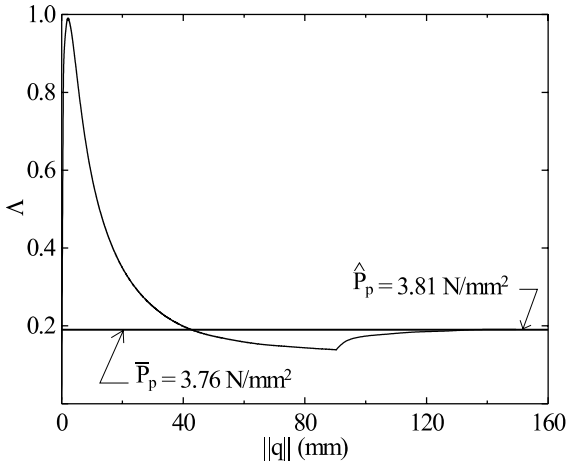

Fig. 10. Load intensity factor versus displacement vector norm of model TSP24B.

Table 3
Experimental $\hat{P}_p$ and numerical $\overline{P}_p$ results of propagation pressure in small scale models

Model	$\hat{P}_p$ (N/mm²)	$\overline{P}_p$ (N/mm²)	Difference (%)
TSP16A	14.38	14.14	−1.67
TSP16B	11.72	11.95	1.96
TSP21A	5.01	4.37	−12.77
TSP21B	5.08	4.88	−3.94
TSP24A	4.31	4.86	12.76
TSP24A	3.81	3.76	−1.31

5. Concluding remarks

Theoretical and numerical procedures have been successfully proposed for the simulation of the buckle propagation phenomenon in deepwater pipelines. A computer program based on both finite difference method and dynamic relaxation technique has been implemented to solve the thin shell equations taking into account geometrically nonlinear behavior and plasticity in the post-buckling regime.

Sanders' thin shell equations were explicitly presented through ordinary notation using lines of curvatures for coordinates, which can be useful to solve problems related to general shell structures under following forces, finite displacements and small strains.

The solution procedure used in the post-buckling regime combined the explicit dynamic relaxation technique to the arc-length method. It proved to be an useful numerical tool to solve structural problems involving several nonlinearities. It can be easily vectorized using adequate computer languages, which provides a fast and reliable approach to analyze post-buckling behavior of nonlinear structures.

Correlation between numerical and experimental results for small scale steel tubes presented good agreement. Additional tests on full-scale pipes are recommended in order to provide additional results for a conclusive correlation study and confidence for using the proposed software in the design of deepwater pipelines.

Acknowledgements

The authors would like to acknowledge the financial support from PETROBRAS, CAPES, CNPq, FAPERJ and the programs RECOPE and PRONEX from the Brazilian Ministry of Science and Technology for supporting different phases of the research conducted on deepwater pipelines at COPPE – Submarine Technology Laboratory.

Appendix A. Definition of total strain

A natural definition of strain ($\varepsilon_{\alpha\beta}$) at a shell generic point is given by the following expression:

$$\varepsilon_{\alpha\beta} = \frac{1}{2}(G_{\alpha\beta} - g_{\alpha\beta}), \tag{A.1}$$

where $g_{\alpha\beta}$ and $G_{\alpha\beta}$ are the covariant metric tensors of the parallel surfaces for the undeformed and deformed middle surface, respectively. They are defined through the expressions

$$g_{\alpha\beta} = \boldsymbol{g}_\alpha \cdot \boldsymbol{g}_\beta \quad \text{and} \quad G_{\alpha\beta} = \boldsymbol{G}_\alpha \cdot \boldsymbol{G}_\beta, \tag{A.2}$$

where $\boldsymbol{g}_\alpha$ and $\boldsymbol{G}_\alpha$ are the base vectors of parallel surfaces to the undeformed and deformed middle surface, respectively. With the aid of the Love–Kirchhoff hypothesis the following two expressions may be written

$$\boldsymbol{r} = \boldsymbol{s} + \xi^3 \boldsymbol{a}_3 \quad \text{and} \quad \boldsymbol{R} = \boldsymbol{S} + \xi^3 \boldsymbol{A}_3, \tag{A.3}$$

where $\boldsymbol{r}$ is the position vector of a generic point P at the undeformed shell, $\boldsymbol{s}$ is the position vector of its orthogonal projection on the undeformed middle surface, $\boldsymbol{a}_3$ is the normal unit vector at P and ξ^3 the normal coordinate. The symbols $\boldsymbol{R}$, $\boldsymbol{S}$ and $\boldsymbol{A}_3$ represent the analogous quantities related to the deformed shell. Partial derivatives of Eq. (A.3) in relation to the middle surface curvilinear coordinate ξ^α leads to

$$\boldsymbol{r}_{,\alpha} = \boldsymbol{s}_{,\alpha} + \xi^3 \boldsymbol{a}_{3,\alpha} \quad \text{and} \quad \boldsymbol{R}_{,\alpha} = \boldsymbol{S}_{,\alpha} + \xi^3 \boldsymbol{A}_{3,\alpha}. \tag{A.4}$$

With the aid of the definitions of base vectors and curvature tensors, Eq. (A.4) are rewritten as

$$\boldsymbol{g}_\alpha = \boldsymbol{a}_\alpha + \xi^3 b_\alpha^\beta \boldsymbol{a}_\beta \quad \text{and} \quad \boldsymbol{G}_\alpha = \boldsymbol{A}_\alpha + \xi^3 B_\alpha^\beta \boldsymbol{A}_\beta, \tag{A.5}$$

where $\boldsymbol{a}_\alpha$ and b_α^β are, respectively, the base vectors and the curvature mixed tensor of the undeformed middle surface, while $\boldsymbol{A}_\alpha$ and B_α^β refer to the deformed middle surface. Therefore, the base vectors $\boldsymbol{G}_\alpha$ and $\boldsymbol{g}_\alpha$ may be expressed as

$$\boldsymbol{g}_\alpha = \mu_\alpha^\beta \boldsymbol{a}_\beta \quad \text{and} \quad \boldsymbol{G}_\alpha = M_\alpha^\beta \boldsymbol{A}_\beta, \tag{A.6}$$

where

$$\mu_\alpha^\beta = \delta_\alpha^\beta + \xi^3 b_\alpha^\beta \quad \text{and} \quad M_\alpha^\beta = \delta_\alpha^\beta + \xi^3 B_\alpha^\beta. \tag{A.7}$$

From the equations above the total strain can be rewritten as,

$$\begin{aligned}
\varepsilon_{\alpha\beta} &= \frac{1}{2}\left(\boldsymbol{G}_\alpha \cdot \boldsymbol{G}_\beta + \boldsymbol{g}_\alpha \cdot \boldsymbol{g}_\beta\right) = \frac{1}{2}\left(M_\alpha^\gamma M_\beta^\lambda A_{\gamma\lambda} - \mu_\alpha^\gamma \mu_\beta^\lambda a_{\gamma\lambda}\right) \\
&= \frac{1}{2}\left\{\left[\delta_\alpha^\gamma \delta_\beta^\lambda + \xi^3 \delta_\alpha^\gamma B_\beta^\lambda + \xi^3 \delta_\beta^\lambda B_\alpha^\gamma + \left(\xi^3\right)^2 B_\alpha^\gamma B_\beta^\lambda\right] A_{\gamma\lambda} + \left[\delta_\alpha^\gamma \delta_\beta^\lambda + \xi^3 \delta_\alpha^\gamma b_\beta^\lambda + \xi^3 \delta_\beta^\lambda b_\alpha^\gamma + \left(\xi^3\right)^2 b_\alpha^\gamma b_\beta^\lambda\right] a_{\gamma\lambda}\right\} \\
&= \frac{1}{2}\left(A_{\alpha\beta} - a_{\alpha\beta}\right) + \left(B_{\alpha\beta} - b_{\alpha\beta}\right)\xi^3 + \frac{1}{2}\left(A_{\gamma\lambda} B_\alpha^\gamma B_\beta^\lambda - a_{\gamma\lambda} b_\alpha^\gamma b_\beta^\lambda\right)\left(\xi^3\right)^2 \\
&= E_{\alpha\beta} + K_{\alpha\beta}\xi^3 + \frac{1}{2}\left(A_{\gamma\lambda} B_\alpha^\gamma B_\beta^\lambda - a_{\gamma\lambda} b_\alpha^\gamma b_\beta^\lambda\right)\left(\xi^3\right)^2,
\end{aligned} \tag{A.8}$$

where $a_{\alpha\beta}$ and $A_{\alpha\beta}$ are respectively the metric tensors of the undeformed and deformed middle surface and the natural definitions of the tensors $E_{\alpha\beta}$ and $K_{\alpha\beta}$ were applied as follow

$$A_{\alpha\gamma} a^{\gamma\beta} = 2E_{\alpha\gamma} a^{\gamma\beta} + \delta_\alpha^\beta \quad \text{and} \quad b_\alpha^\beta = \left(B_{\alpha\gamma} - K_{\alpha\gamma}\right) a^{\gamma\beta}. \tag{A.9}$$

The fourth term of the last member in Eq. (A.8) can be rewritten as

$$\begin{aligned}
a_{\gamma\lambda} b_\alpha^\gamma b_\beta^\lambda &= a_{\gamma\lambda}\left(B_{\alpha\rho} - K_{\alpha\rho}\right) a^{\rho\gamma}\left(B_{\beta\mu} - K_{\beta\mu}\right) a^{\mu\lambda} \\
&= a^{\rho\mu}\left(A_{\lambda\rho} B_\alpha^\lambda B_\beta^\delta A_{\delta\mu} - A_{\lambda\rho} B_\alpha^\lambda K_{\beta\mu} - A_{\lambda\mu} B_\beta^\lambda K_{\alpha\rho} + K_{\alpha\rho} K_{\beta\mu}\right) \\
&= \left(2E_{\lambda\rho} a^{\rho\mu} + \delta_\lambda^\mu\right)\left[\left(B_\alpha^\lambda B_\beta^\delta A_{\delta\mu}\right) - \left(B_\alpha^\lambda K_{\beta\mu}\right)\right] - \left(2E_{\lambda\mu} a^{\mu\rho} + \delta_\lambda^\rho\right) B_\beta^\lambda K_{\alpha\rho} \\
&= 2A_{\delta\mu} a^{\rho\mu} E_{\lambda\rho} B_\alpha^\lambda B_\beta^\delta + B_\alpha^\mu B_\beta^\delta A_{\mu\delta} - B_\alpha^\mu K_{\mu\beta} - B_\beta^\rho K_{\rho\alpha} \\
&= 2E_{\lambda\rho} B_\alpha^\lambda B_\beta^\rho + B_\alpha^\mu B_\beta^\delta A_{\mu\delta} - B_\alpha^\mu K_{\mu\beta} - B_\beta^\rho K_{\rho\alpha},
\end{aligned}$$

where the products of strains were neglected and the indexes of tensors components $B_{\alpha\beta}$ were raised by the metrics $A^{\alpha\beta}$. Returning this term to Eq. (A.8) the following expression is obtained

$$\varepsilon_{\alpha\beta} = E_{\alpha\beta} + K_{\alpha\beta}\xi^3 + \frac{1}{2}\left(A_{\gamma\lambda} B_\alpha^\gamma B_\beta^\lambda - 2E_{\lambda\rho} B_\alpha^\lambda B_\beta^\rho - A_{\mu\delta} B_\alpha^\mu B_\beta^\delta + B_\alpha^\mu K_{\mu\beta} + B_\beta^\rho K_{\rho\alpha}\right)\left(\xi^3\right)^2$$

and finally,

$$\varepsilon_{\alpha\beta} = E_{\alpha\beta} + K_{\alpha\beta}\xi^3 + \frac{1}{2}\left(B_\alpha^\gamma K_{\gamma\beta} + B_\beta^\gamma K_{\gamma\alpha} - 2E_{\gamma\delta} B_\alpha^\gamma B_\beta^\delta\right)\left(\xi^3\right)^2. \tag{A.10}$$

This equation was used by Koiter (1970) to represent virtual strains on parallel surfaces to the deformed middle surface. It is applicable to general thin shells assuming finite displacements and small strains. The use of Love–Kirchhoff assumptions in Eq. (A.1) resulted in an expression defined as a function of the second order symmetric tensors $E_{\alpha\beta}$ and $K_{\alpha\beta}$ corresponding to the shell membrane and bending strains.

In order to specialize the above equation to the geometry studied, the Greek symbols assume values 1 and 2 corresponding to the curvilinear coordinates x and θ in a circular cylindrical shell. Thus, the components of the total strain expressed in ordinary notation are obtained from Eq. (A.10) as:

$$\varepsilon_{xx} = E_{xx} + K_{xx}z, \tag{A.11}$$

$$\varepsilon_{\theta\theta} = \left[E_{\theta\theta} + K_{\theta\theta}z + \left(K_{\theta\theta} - \frac{E_{\theta\theta}}{R}\right)\frac{z^2}{R}\right] \Big/ \left(1 + \frac{z}{R}\right)^2 \tag{A.12}$$

and

$$\varepsilon_{x\theta} = \left[E_{x\theta} + K_{x\theta}z + K_{x\theta}\frac{z^2}{2R}\right] \Big/ \left(1 + \frac{z}{R}\right). \tag{A.13}$$

Appendix B. Kinematic relations

The general thin shell equations for membrane and bending strain components (Sanders, 1963) are presented in ordinary notation assuming finite displacements, small strains and constant Lamé coefficients A_1 and A_2.

$$E_{11} = \frac{1}{2}\left(\lambda_{11}^2 + \lambda_{21}^2 + \mu_1^2 - 1\right), \tag{B.1}$$

$$E_{12} = \frac{1}{2}\left(\lambda_{11}\lambda_{12} + \lambda_{22}\lambda_{21} + \mu_1\mu_2\right), \tag{B.2}$$

$$K_{11} = \left(\frac{1}{R_1}\lambda_{11} - \frac{1}{A_1}\mu_{1,1}\right)\cos\omega - \left(\frac{1}{A_1}\lambda_{11,1} + \frac{1}{R_1}\mu_1\right)v_1 - \frac{1}{A_1}\lambda_{21,1}v_2 - \frac{1}{R_1} \tag{B.3}$$

and

$$K_{12} = \left(\frac{1}{R_2}\lambda_{21} - \frac{1}{A_2}\mu_{1,2}\right)\cos\omega - \frac{1}{A_2}\lambda_{11,2}v_1 - \left(\frac{1}{A_2}\lambda_{21,2} + \frac{1}{R_2}\mu_1\right)v_2, \tag{B.4}$$

where

$$\lambda_{11} = 1 + \frac{1}{A_1}u_{1,1} + \frac{1}{R_1}w, \tag{B.5}$$

$$\lambda_{12} = \frac{1}{A_2}u_{1,2}, \tag{B.6}$$

$$\mu_1 = \frac{1}{A_1}w_{,1} - \frac{1}{R_1}u_1, \tag{B.7}$$

$$v_1 = \left(\lambda_{21}\mu_2 - \lambda_{22}\mu_1\right), \tag{B.8}$$

$$\cos\omega = \left(\lambda_{11}\lambda_{22} - \lambda_{12}\lambda_{21}\right), \tag{B.9}$$

R_1 and R_2 are the principal radii of curvature, u_α and w are respectively, the tangential and normal displacements of the middle surface and the comma means partial derivatives in relation to the curvilinear coordinates ξ_1 and ξ_2. Here and below in Appendix C the missing equations are obtained by interchanging subscripts 1 and 2.

The components of both membrane and bending strain tensors for circular cylindrical shells are obtained from Eqs. (B.1)–(B.9) as:

$$E_{xx} = \frac{\partial u}{\partial x} + \frac{1}{2}\left[\left(\frac{\partial u}{\partial x}\right)^2 + \left(\frac{\partial v}{\partial x}\right)^2 + \left(\frac{\partial w}{\partial x}\right)^2\right], \tag{B.10}$$

$$E_{\theta\theta} = \frac{1}{R}\left(\frac{\partial v}{\partial \theta} + w\right) + \frac{1}{2}\left(\frac{1}{R}\frac{\partial u}{\partial \theta}\right)^2 + \frac{1}{2R^2}\left(\frac{\partial v}{\partial \theta} + w\right)^2 + \frac{1}{2R^2}\left(\frac{\partial w}{\partial \theta} - v\right)^2, \tag{B.11}$$

$$E_{x\theta} = \frac{1}{2}\left[\frac{1}{R}\frac{\partial u}{\partial \theta} + \frac{\partial v}{\partial x} + \frac{1}{R}\frac{\partial u}{\partial x}\frac{\partial u}{\partial \theta} + \frac{1}{R}\frac{\partial v}{\partial x}\left(\frac{\partial v}{\partial \theta} + w\right) + \frac{1}{R}\frac{\partial w}{\partial x}\left(\frac{\partial w}{\partial \theta} - v\right)\right], \tag{B.12}$$

$$K_{xx} = -\left(\frac{\partial^2 u}{\partial x^2}N_1 + \frac{\partial^2 v}{\partial x^2}N_2 + \frac{\partial^2 w}{\partial x^2}N_3\right), \tag{B.13}$$

$$K_{\theta\theta} = -\frac{1}{R^2}\left[\frac{\partial^2 u}{\partial \theta^2}N_1 + \left(\frac{\partial^2 v}{\partial \theta^2} + 2\frac{\partial w}{\partial \theta} - v\right)N_2 + \left(\frac{\partial^2 w}{\partial \theta^2} - 2\frac{\partial v}{\partial \theta} - w - R\right)N_3 + R\right] \tag{B.14}$$

and

$$K_{x\theta} = -\frac{1}{R}\left[\frac{\partial^2 u}{\partial x \partial \theta}N_1 + \left(\frac{\partial^2 v}{\partial x \partial \theta} + \frac{\partial w}{\partial x}\right)N_2 + \left(\frac{\partial^2 w}{\partial x \partial \theta} - \frac{\partial v}{\partial x}\right)N_3\right], \tag{B.15}$$

where N_1, N_2 and N_3 are the local components of the unit vector normal to the deformed middle surface in axial, hoop and radial directions, respectively,

$$N_1 = \frac{1}{R}\frac{\partial v}{\partial x}\left(\frac{\partial w}{\partial \theta} - v\right) - \frac{1}{R}\frac{\partial w}{\partial x}\left(\frac{\partial v}{\partial \theta} + w\right) - \frac{\partial w}{\partial x}, \tag{B.16}$$

$$N_2 = -\frac{1}{R}\frac{\partial u}{\partial x}\left(\frac{\partial w}{\partial \theta} - v\right) - \frac{1}{R}\left(\frac{\partial w}{\partial \theta} - v\right) + \frac{1}{R}\frac{\partial w}{\partial x}\frac{\partial u}{\partial \theta} \tag{B.17}$$

and

$$N_3 = 1 + \frac{\partial u}{\partial x} + \frac{1}{R}\left(\frac{\partial v}{\partial \theta} + w\right) + \frac{1}{R}\frac{\partial u}{\partial x}\left(\frac{\partial v}{\partial \theta} + w\right) - \frac{1}{R}\frac{\partial v}{\partial x}\frac{\partial u}{\partial \theta}. \tag{B.18}$$

Appendix C. Modified equilibrium equations

Sanders' equations are based on dead-loading and are therefore inadequate for applications including large rotations where the acting pressure remains normal to the deformed middle surface. In order to take into account the following force type of loading it is necessary to use the components of the unit vector normal to the deformed middle surface represented by Eqs. (B.8) and (B.9). The external fluid pressure (p) is multiplied by the local components v_1, v_2 and $\cos\omega$, being added to the respective force equilibrium equations to provide the following forces. Therefore, the equations for resultant forces and moments applicable to general thin shells assuming constant Lamé coefficients and small strains are:

$$A_2(\lambda_{11}N_{11})_{,1} + A_1(\lambda_{11}N_{12})_{,2} + A_2(\lambda_{12}N_{12})_{,1} + A_1(\lambda_{12}N_{22})_{,2} + A_2(\lambda_{11}B_{11}M_{11})_{,1} + A_2(\lambda_{12}B_{12}M_{11})_{,1} + A_2(\lambda_{11}B_{12}M_{12})_{,1} + A_2(\lambda_{12}B_{22}M_{12})_{,1} + A_1(\lambda_{11}B_{11}M_{12})_{,2} + A_1(\lambda_{12}B_{12}M_{12})_{,2} + A_1(\lambda_{11}B_{12}M_{22})_{,2} + A_1(\lambda_{12}B_{22}M_{22})_{,2} + \frac{A_1A_2}{R_1}(\mu_1N_{11} + \mu_2N_{12}) + \frac{A_1A_2}{R_1}(\mu_1B_{11} + \mu_2B_{12})M_{11} + \frac{A_1A_2}{R_1}(\mu_1B_{12} + \mu_2B_{22})M_{12} + A_2(v_1Q_1)_{,1} + A_1(v_1Q_2)_{,2} + \frac{A_1A_2}{R_1}\cos\omega Q_1 - A_1A_2v_1p = 0, \tag{C.1}$$

$$A_2(\mu_1N_{11})_{,1} + A_1(\mu_1N_{12})_{,2} + A_2(\mu_2N_{12})_{,1} + A_1(\mu_2N_{22})_{,2} + A_2(\mu_1B_{11}M_{11})_{,1} + A_2(\mu_2B_{12}M_{11})_{,1} + A_2(\mu_1B_{12}M_{12})_{,1} + A_2(\mu_2B_{22}M_{12})_{,1} + A_1(\mu_2B_{22}M_{22})_{,2} + A_1(\mu_1B_{12}M_{22})_{,2} + A_1(\mu_2B_{12}M_{12})_{,2} + A_1(\mu_1B_{11}M_{12})_{,2} - \frac{A_1A_2}{R_1}[(\lambda_{11}N_{11} + \lambda_{12}N_{12}) + (\lambda_{11}B_{11}M_{11} + \lambda_{11}B_{12}M_{12} + \lambda_{12}B_{12}M_{11} + \lambda_{12}B_{22}M_{12})] - \frac{A_1A_2}{R_2}[(\lambda_{22}N_{22} + \lambda_{21}N_{12}) + (\lambda_{22}B_{22}M_{22} + \lambda_{22}B_{12}M_{12} + \lambda_{21}B_{12}M_{22} + \lambda_{21}B_{11}M_{12})] + A_2(\cos\omega Q_1)_{,1} + A_1(\cos\omega Q_2)_{,2} - \frac{A_1A_2}{R_1}v_1Q_1 - \frac{A_1A_2}{R_2}v_2Q_2 - A_1A_2\cos\omega p = 0 \tag{C.2}$$

and

$$A_2M_{11,1} + A_1M_{12,2} - A_1A_2Q_1 = 0, \tag{C.3}$$

where

$$B_{11} = K_{11} + 1/R_1 \tag{C.4}$$

and

$$B_{12} = K_{12}. \tag{C.5}$$

Both stress and bending moment resultants are the modified tensors of Eqs. (5) and (6) while Q_α is the transverse shear resultant.

References

Cassel, A.C., Hobbs, R.A., 1976. Numerical stability of dynamic relaxation analysis of non-linear structures. International Journal for Numerical Methods in Engineering 10, 1407–1410.

Charter, E., Hutchinson, J.W., 1984. On the propagation of bulges and buckles. Transactions of the ASME, Journal of Applied Mechanics 51, 269–277.

Crisfield, M.A., 1981. A fast incremental/iterative solution procedure that handles snap-through. Computers and Structures 13, 55–62.

Crisfield, M.A., 1991. Non-linear finite element analysis of solids and structures. Essentials, first ed. vol. 1. Wiley, New York.

Dyau, J.Y., Kyriakides, S., 1993. On the propagation pressure of long cylindrical shells under external pressure. International Journal of Mechanical Sciences 35 (8), 675–713.

Estefen, S.F., Aguiar, L.A.D., 1994. Experimental evaluation of the propagation pressure of steel small scale models. Coppetec Report ET-170216, COPPE/UFRJ, Rio de Janeiro, RJ, Brazil (in Portuguese).

Estefen, S.F., Aguiar, L.A.D., Alves, T.M.J., 1996. Correlation between analytical and experimental results for propagation buckling. Proceedings of the 15th International Conference on Offshore Mechanics and Arctic Engineering, vol. 5. Florence, Italy, pp. 187–193.

Jensen, H.M., 1988. Collapse of hydrostatically loaded cylindrical shells. International Journal of Solids and Structures 24 (1), 51–64.

Johns, T.G., Mesloh, R.E., Sorenson, J.E., 1976. Propagating buckle arrestors for offshore pipelines. Offshore Technology Conference, Houston, Texas, USA.

Kamalarasa, S., Calladine, C.R., 1988. Buckle propagation in submarine pipelines. International Journal on Mechanical Sciences 30, 217–228.

Koiter, W.T., 1970. On the foundations of the linear theory of thin elastic shells I, II. Proceedings of the Koninklijke Nederlandse Akademie Van Wetenschappen, series b, 73, 169–195.

Kyriakides, S., Babcock, C.D., 1979. On the dynamics and the arrest of the propagating buckle in offshore pipelines. Offshore Technology Conference, Houston, Texas, USA.

Kyriakides, S., Babcock, C.D., 1980a. On the slip-on buckle arrestor for offshore pipelines. Offshore Technology Conference, Houston, Texas, USA.

Kyriakides, S., Babcock, C.D., 1980b. The spiral arrestor – a new buckle arrestor design for offshore pipelines. Transactions of the ASME, Journal of Pressure Vessel Technology 102, 188–193.

Kyriakides, S., Babcock, C.D., 1981. Experimental determination of the propagation pressure of circular pipes. Transactions of the ASME, Journal of Pressure Vessel Technology 103, 328–336.

Kyriakides, S., Yeh, M.K., Roach, D., 1984. On the determination of the propagation pressure of long circular tubes. Transactions of the ASME, Journal of Pressure Vessel Technology 106, 150–159.

Kyriakides, S., Chang, Y.C., 1992. On the effect of axial tension on the propagation pressure of long cylindrical shells. International Journal of Mechanical Sciences 34 (1), 3–15.

Kyriakides, S., 1994. Propagating instabilities in structures. Advances in Applied Mechanics 30, 67–189.

Mesloh, R.E., Sorenson, J.E., Atterbury, T.J., 1973. Buckling and offshore pipelines. Gas Magazine 7, 40–43.

Mesloh, R.E., Johns, T.G., Sorenson, J.E., 1976. The propagating buckle. Proceedings of the International Conference on Behaviour of Offshore Structures, vol. 1. USA, pp. 787–797.

Palmer, A.C., 1975. Buckle propagation in submarine pipelines. Nature 254 (5495), 46–48.

Pasqualino, I.P., 1998. Buckle propagation of hydrostatically loaded cylindrical shells. D.Sc. Dissertation Thesis, COPPE/UFRJ, Rio de Janeiro, RJ, Brazil (in Portuguese).

Ramesh, G., Krishnamoorthy, C.S., 1993. Post-buckling analysis of structures by dynamic relaxation. International Journal for Numerical Methods in Engineering 36, 1339–1364.

Riks, E., 1970. On the numerical solution of snapping problems in the theory of elastic stability. Ph.D. Dissertation Thesis, SUDAAR 401, Department of Aero/Astronautics, Stanford University, Stanford, California, USA.

Riks, E., 1979. An incremental approach to the solution of snapping and buckling problems. International Journal of Solids and Structures 15 (7), 529–551.

Sanders, J.L., 1963. Nonlinear theories of thin shells. Quarterly of Applied Mathematics 21 (1), 21–36.

Song, H.W., Tassoulas, J.L., 1991. Dynamics of propagating buckles in deep-water pipelines. Proceedings of Offshore Mechanics and Arctic Engineering Conference. ASME, vol. 5. Stavanger, Norway, pp. 187–192.

Steel, W.J.M., Spence, J., 1983. On propagating buckles and their arrest in sub-sea pipelines. Proceedings of the Institution of Mechanical Engineers 197A, 139–147.

Tassoulas, J.L., Katsounas, A.T., Song, H.W., 1990. Finite element analysis of propagating buckles in deepwater pipelines. Offshore Technology Conference, Houston, Texas, USA.

Underwood, P., 1983. Dynamic relaxation. In: Belytschko T., Hughes T.J.R. (Eds.), Computational Methods for Transient Analysis. North-Holland, Amsterdam, pp. 245–265.

Wempner, G.A., 1971. Discrete approximations related to nonlinear theories of solids. International Journal of Solids and Structures 7, 1581–1599.